Unveiling the singular dynamics in the cosmic large-scale structure

Cornelius Rampf, Uriel Frisch, Oliver Hahn

Monthly Notices of the ROYAL ASTRONOMICAL SOCIETY

MNRAS **505,** L90–L94 (2021) https://doi.org/10.1093/mnrasl/slab053
Advance Access publication 2021 May 25

Unveiling the singular dynamics in the cosmic large-scale structure

Cornelius Rampf [1]★ Uriel Frisch [1] and Oliver Hahn [1,2,3]

[1]*Observatoire de la Côte d'Azur, CNRS, Laboratoire Lagrange, Université Côte d'Azur, Boulevard de l'Observatoire, CS 34229, F-06304 Nice, France*
[2]*Department of Astrophysics, University of Vienna, Türkenschanzstraße 17, A-1180 Vienna, Austria*
[3]*Department of Mathematics, University of Vienna, Oskar-Morgenstern-Platz 1, A-1090 Vienna, Austria*

Accepted 2021 May 19. Received 2021 April 24; in original form 2021 January 29

ABSTRACT

It is known that the gravitational collapse of cold dark matter leads to infinite-density caustics that seed the primordial dark-matter haloes in the large-scale structure. The development of these caustics begins, generically, as an almost one-dimensional phenomenon with the formation of pancakes. Focusing on the one-dimensional case, we identify a landscape of non-differentiable, and thus, singular features in the particle acceleration that emerge after the first crossing of particle trajectories. We complement our fully analytical studies by high-resolution simulations and find outstanding agreement, particularly shortly after the first crossing. We develop the methods in one space dimension but outline briefly the necessary steps for the 3D case.

Key words: instabilities – cosmology: theory – dark matter – large-scale structure of Universe.

1 INTRODUCTION

A simple example of a singularity is when a function $\xi(\tau)$ has local behaviour $\propto(\tau - \tau_1)^\lambda$ around τ_1, where $\lambda \notin \mathbb{N}$ is the singularity exponent. If λ is a negative integer, then the singularity has a simple pole-like structure. If λ is instead a positive non-integer number, then certain derivatives of $\xi(\tau)$ will blow up around τ_1 and, as a result, $\xi(\tau)$ cannot be represented locally by a Taylor series.

In cosmology, the obvious singularities are density caustics that comprise the central building block for the cosmic large-scale structure. At the particle level, infinite-density caustics result from shell-crossing, the crossing of cold dark matter (CDM) trajectories. Once particles have crossed for the first time, the single-stream flow becomes multistream. Subsequently, secondary gravitational infall commences, inducing more shell-crossings that lead to a proliferation of streams, and eventually to virialized structures.

Some of the singularities were classified by Arnol'd (1980), Arnold, Shandarin & Zeldovich (1982), by exploiting an approximate non-linear theory of gravitational instability, the Zel'dovich approximation (ZA; Zel'dovich 1970). However, singularities in derivatives of the particle trajectories, which we report here, remained undetected as the ZA is an acceleration-free model for non-linear collapse, thereby being effectively blind to secondary gravitational infall.

Central to the analysis of Arnol'd (1980), Arnold et al. (1982), as well as ours, is the use of Lagrangian-coordinates approaches to gravitational instability that permits investigating singularities in a tractable manner. The ZA is the lowest-order Lagrangian-coordinates approximation to the cosmological fluid equations (the single-stream case of the Vlasov–Poisson equations). Furthermore, it is exact in 1D (Novikov 1969), as long as multistream flow has not yet appeared. Beyond 1D, higher order approximations should be incorporated, and the corresponding framework is dubbed Lagrangian perturbation theory (LPT; Buchert & Götz 1987; Bouchet et al. 1992; Buchert 1992; Ehlers & Buchert 1997; Bernardeau et al. 2002; Rampf & Buchert 2012; Zheligovsky & Frisch 2014). In LPT the displacement field is the only dynamical variable, which is expanded as a (temporal or spatial) Taylor series. Recently, the first non-trivial shell-crossing solutions in LPT have been identified (Rampf & Frisch 2017; Rampf 2019), while numerical evidence of convergence of LPT in 3D at shell-crossing was given by Saga, Taruya & Colombi (2018), and Rampf & Hahn (2020).

None the less, the standard implementation of LPT cannot predict secondary gravitational infall, since it is based on a fluid description that does not incorporate multistreaming. Instead, the multistreaming evolution of CDM is governed by the Vlasov–Poisson equations. Following in the footsteps of Colombi (2015), Taruya & Colombi (2017), and Pietroni (2018), here we develop a Lagrangian-coordinates approach for Vlasov–Poisson and detect so far unknown singularities. These singularities comprise the intrinsic reason why standard perturbative techniques based on Taylor expansions break down at shell-crossing, while density singularities could be circumvented using suitable (Lagrangian) coordinates. For simplicity, we assume a 1D (spatial) universe; the corresponding solutions play an important role in 3D cosmology, mainly because shell-crossings generically begin as almost 1D phenomena with the formation of pancakes (e.g. Melott & Shandarin 1989). Notwithstanding, our theoretical tools are scalable to any dimensions with only mild modifications.

2 SET-UP

We denote by $q \mapsto x(q, \tau)$ the Lagrangian map from initial ($\tau = 0$) position q to current position x at time τ, where τ is not the cosmic time t but is proportional to $t^{2/3}$. For simplicity, we assume a spatially flat and matter dominated Einstein–de Sitter (EdS) universe. We make use of comoving coordinates $x = r/a$, where r is the proper space coordinate and a is the cosmic scale factor (for EdS: $a = \tau$).

★ E-mail: cornelius.rampf@oca.eu

The velocity is expressed in terms of the convective time derivative of the map, i.e. $v(x(q,\tau)) = \partial_\tau x(q,\tau) =: \dot{x}(q,\tau)$. The Vlasov–Poisson equations for CDM are

$$\ddot{x} + \frac{3}{2\tau}\dot{x} = -\frac{3}{2\tau}\nabla_x\varphi, \qquad \nabla_x^2\varphi = \frac{\delta(x(q,\tau))}{\tau}, \tag{1}$$

where $\delta := (\rho - \bar{\rho})/\bar{\rho}$ is the dimensionless density contrast. Note that $\dot{x} = v = u/\partial_t a$ (where u is the standard peculiar velocity) has units of lengths due to the use of a dimensionless time variable $\tau = a$; for simplicity, since no physical scales are introduced in an EdS universe, we set from here on all units to unity.

Both numerical N-body methods and theory aim to solve equation (1), however with at least one substantial difference, namely that in N-body methods the density contrast is determined by using an N-particle approximation. By contrast, in theory one can determine the density using (Taylor & Hamilton 1996)

$$\delta\big(x(q,\tau)\big) = \int \delta_{\rm D}\big[x(q,\tau) - x(q',\tau)\big]\,{\rm d}q' - 1, \tag{2}$$

where '$\delta_{\rm D}$' is the Dirac-delta.

Observe that equation (1) is invariant under the non-Galilean coordinate transformation $x \to x + \zeta_0(\tau)$, where ζ_0 is an arbitrary function of time (Heckmann & Schücking 1955; Ehlers & Buchert 1997). We use this symmetry to enforce the following centre-of-mass condition for the Lagrangian displacement field $\xi(q,\tau) := x(q,\tau) - q$ on the torus $\mathbb{T}$,

$$\int_{\mathbb{T}} \xi(q',\tau)\,{\rm d}q' = 0, \qquad \forall\ \tau > 0. \tag{3}$$

Note that periodic boundary conditions are assumed in this letter.

3 SOLUTION STRATEGY AND INITIAL DATA

Following a standard procedure (e.g. Bernardeau et al. 2002), equations (1) and (2) can be combined into a single equation by first taking the Eulerian (or Lagrangian) divergence of the former. Converting the derivatives according to $(\partial_q x)\,\partial_x = \partial_q$, we obtain

$$\partial_q \mathfrak{R}_\tau \xi = -\frac{3}{2}F(x(q,\tau)), \tag{4}$$

where $\mathfrak{R}_\tau = \tau^2\partial_\tau^2 + (3\tau/2)\partial_\tau - 3/2$ is the linear growth operator with eigenvalues $+1$ and $-3/2$, and

$$F(x(q,\tau)) := (\partial_q x)\int \delta_{\rm D}[x(q,\tau) - x(q',\tau)]\,{\rm d}q' - 1, \tag{5}$$

is the effective multistream force ($F = 0$ in single-stream regions). See the supplementary material A1 for derivations. Integrating equation (4) in space from 0 to q, we obtain our main evolution equation

$$\mathfrak{R}_\tau\,\{\xi(q,\tau) - \xi_{\rm c}(\tau)\} = -\frac{3}{2}S(x(q,\tau)). \tag{6}$$

Here, $S(x(q,\tau)) := \int_0^q F(x(q',\tau))\,{\rm d}q'$ is the integrated multistreaming force, while $\xi_{\rm c}(\tau) := \xi(q = 0,\ \tau)$ is a space-independent integration constant which, as we show, needs to be adjusted due to multistreaming by virtue of equation (3), such that equations (1) and (6) agree with each other.

To solve equation (6), we provide growing-mode initial conditions at $\tau = 0$. We specify, actually without loss of generality (see supplementary material A2), the initial velocity to be periodic,

$$\dot{\xi}(q,\tau=0) = -\sin q + c\sin^4 q - \frac{6c}{5}\sin^6 q =: v^{\rm (ini)}, \tag{7}$$

where c is a free parameter, and we have added a counter term $\propto \sin^6 q$ to avoid trivial violations of equation (3). In the real Universe, the initial velocity is of random nature, which however may be locally expanded as $v^{\rm ini} = -aq + bq^3 + cq^4 + \ldots$, where a – c are free parameters that do not alter the nature of the reported singularities, and we have removed a quadratic term by a Galilean transformation. We will see shortly that such low-order truncations allow us to accurately determine the post-shell-crossing forces by analytical means. Note that the setting $c = 0$, as effectively employed by Taruya & Colombi (2017), enforces a perfectly point-symmetric collapse which we claim, however, is degenerate in a Universe with random initial conditions. Therefore, we keep c non-zero but assume for the simplicity that it is sufficiently small ($c \lesssim 0.49$), ensuring that the location of the first shell-crossing, controlled by the minimum of $\partial_q v^{\rm (ini)}$, occurs at the origin $q = 0$ in our chosen coordinate system.

4 SHELL-CROSSING SOLUTION

In the single-stream regime, the spatial integral in F simplifies as there is only a single root $x(q,\tau) = x(q',\tau)$ that contributes to the integral, yielding $1/(\partial_q x)$; thus $F = 0$ and so does its integral, $S = 0$. Hence, equation (6) reduces to $\mathfrak{R}_\tau\{\xi - \xi_{\rm c}\} = 0$. Furthermore, due to the absence of asymmetries in the evolution equation, we have, by virtue of the centre-of-mass condition (3), that $\xi_{\rm c} = 0$. Thus, the evolution equation can be solved with the initial condition (7), and we recover the well-known Zel'dovich solution (Zel'dovich 1970)

$$x_{\rm ZA}(q,\tau) = q + \tau\, v^{\rm (ini)}(q). \tag{8}$$

This solution is only valid until the time of first shell-crossing, denoted with $\tau_\star$, that is when the particle trajectory loses its single-valuedness and CDM enters into the multistream regime. For topological reasons (cf. Fig. 1), the first appearance of $\partial_q x_{\rm ZA} = 0$ marks the first shell-crossing, which, as is well known, is accompanied with an infinite density (cf. equation 2):

$$\delta(x_{\rm ZA}(q_\star,\tau_\star)) = \frac{1}{\partial_q x_{\rm ZA}(q,\tau_\star)|_{q=q_\star}} - 1 = \infty. \tag{9}$$

It is easily checked that for the considered initial conditions, the first shell-crossing occurs at $\tau_\star = 1$ at $q = q_\star = 0$, for $c \lesssim 0.49$.

5 POST-SHELL-CROSSING DYNAMICS

To make progress on the analysis after shell-crossing, we introduce an iterative scheme for equation (6) in which the evolution of the post-shell-crossing (PSC) displacement, $\xi_{\rm PSC}$, is driven by an integrated force resulting from the Zel'dovich flow, i.e.

$$\mathfrak{R}_\tau\,\{\xi_{\rm PSC}(q,\tau) - \xi_{\rm c}(\tau)\} = -\frac{3}{2}S_{\rm ZA}(q,\tau) \tag{10}$$

in the first iteration, where $S_{\rm ZA}(q,\tau) := \int_0^q F(x_{\rm ZA}(q',\tau))\,{\rm d}q'$. In the following we summarize the main technical steps to solve equation (10), while in-depth derivations and instructions for higher-order refinements are respectively provided in the supplementary material B and C. We remark that our iterative scheme is related to the one of Taruya & Colombi (2017) but there are differences; see the supplementary material D for details.

We first need to solve for $S_{\rm ZA}$; for this, observe that the force in equation (5) can be written as $F(x(q,\tau)) = \int \partial_q\Theta(x(q,\tau) - x(q',\tau))\,{\rm d}q' - 1$, where Θ is the Heaviside step function. Therefore,

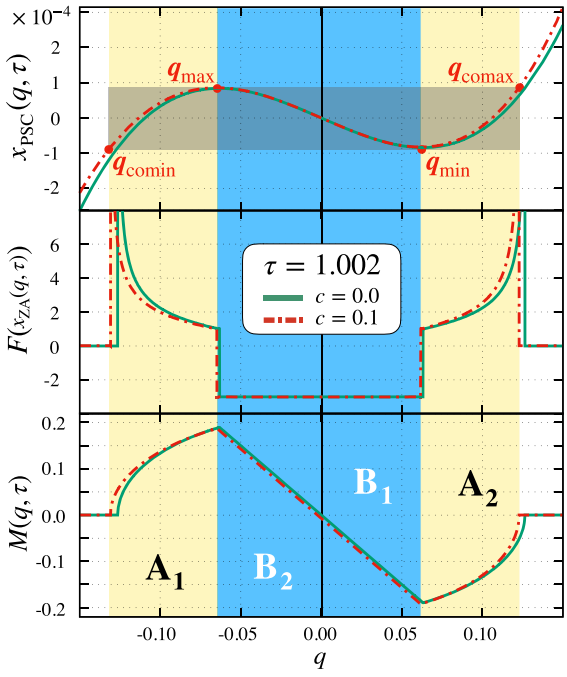

Figure 1. Shown is the post-shell-crossing map $x_{\rm PSC} = q + \xi_{\rm PSC}$ (top panel), the multistreaming force F (middle panel) and $M := S_{\rm ZA} - S_{\rm c}$ (lower panel). All plots are evaluated after the first shell-crossing ($\tau_\star = 1$), namely at $\tau = 1.002$. Green (solid) lines denote $c = 0$, whereas red (dot-dashed) lines $c = 0.1$. The grey (horizontally) shaded region marks the multistreaming region (for $c = 0.1$), which spans up the ascending ($\mathbf{A}_{1,2}$; yellow-shaded) and the descending ($\mathbf{B}_{1,2}$; blue-shaded) multistream regimes. The single-stream regime ($\mathbf{S}_{1,2}$) has no shading; in this context, note that due to the assumed periodicity, that $q \in [-\pi, \pi]$. The sharp non-differentiable features in F and M, as well as the slight shift of F and M in the presence of non-zero c, are physical effects associated to singular behaviour.

the spatial integral of the force from 0 to q, within the ZA, is simply

$$S_{\rm ZA} = \int \left[\Theta(x_{\rm ZA}(q,\tau) - x_{\rm ZA}(q',\tau)) - \Theta(-x_{\rm ZA}(q',\tau))\right] {\rm d}q' - q, \tag{11}$$

where we have used that $x_{\rm ZA}(q = 0, \tau) = 0$. Thus, solving for $S_{\rm ZA}$ amounts to finding the positions (roots) when the arguments of the Θ's change their signs. Shortly after shell-crossing, and given that c is small, both arguments of the Θ's in equation (11) have three physical roots, implying that the flow has entered the three-stream regime (grey shading in Fig. 1).

Furthermore, the multistreaming regime is still confined to small areas around $q = 0 = q_\star$, thus the positions of the three roots can be obtained by considering the low-order truncation $v^{\rm ini} \approx -q + q^3/6 + c\,q^4$ in $x_{\rm ZA}$ (higher-order terms do not change the nature of the reported singularities). For small c, the positions of the three roots are slightly shifted with respect to the $c = 0$ case, which can be determined in perturbation theory, yielding

$$S_{\rm ZA} = S_{\rm c} + \begin{cases} 0; & 0 \le \tau \le \tau_1; \quad \mathbf{S}_{1,2} \\ -{\rm sign}(q)\sqrt{D(q,\tau)}; & \tau_1 \le \tau \le \tau_2; \quad \mathbf{A}_{1,2} \\ -3q - 36c(1 - 1/\tau); & \tau \ge \tau_2; \quad \mathbf{B}_{1,2} \end{cases} \tag{12}$$

where, stemming from the "$q = 0$" part of equation (11),

$$S_{\rm c} = 36c(1 - 1/\tau)\,\Theta(\tau - 1), \tag{13}$$

to first order in c. Here we have defined

$$D(q,\tau) = 24 - 3q^2 - 24/\tau + 24cq(3 - q^2 - 3/\tau), \tag{14}$$

as well as the space-dependent times

$$\tau_1(q) = 8/(8 - q^2 - 5cq^3), \qquad \tau_2(q) = 2/(2 - q^2 - 8cq^3). \tag{15}$$

Conversely, the Lagrangian positions can be expressed by τ_1 and τ_2, respectively leading to $q_{\rm comin/comax} = \mp\sqrt{8(1 - 1/\tau)} - 20c(1 - 1/\tau)$, and $q_{\rm min/max} = \pm\sqrt{2(1 - 1/\tau)} - 8c(1 - 1/\tau)$, to first order in c. Also, we have $x(q_{\rm min/max}) = x(q_{\rm comin/comax})$ by definition, where comin/comax stands for co-minimum/co-maximum.

For convenience, we have marked the positions $q_{\rm comin/comax}$ and $q_{\rm min/max}$ in Fig. 1, where we also show the multistreaming force $F(x_{\rm ZA}(q,\tau)) = \partial_q S_{\rm ZA}$, and the integral $M := S_{\rm ZA} - S_{\rm c}$. Observe the appearance of several non-differential features in $F(x_{\rm ZA}(q,\tau))$ and $S_{\rm ZA}$, indicating singularities; see the following section for a thorough analysis. We also note that the density is infinite at $q_{\rm min/max}$, where $\partial_q x(q)|_{q=q_{\rm min/max}} = 0$, which is well-known; see e.g. Zel'dovich (1970), and Arnold et al. (1982).

Let us first derive $\xi_{\rm c}(\tau)$, which is generally non-zero due to a forcing imbalance. For this we solve equation (10) in the $q = 0$ case, which, using equations (12) and (3), reduces to ($\tau \ge 1$)

$$\mathfrak{R}_\tau \xi_{\rm c}(\tau) = 54c(1 - 1/\tau). \tag{16}$$

Supplemented with the boundary conditions at shell-crossing $\xi_{\rm c}(\tau = 1) = 0 = \dot\xi_{\rm c}(\tau = 1)$, we obtain for the particle that is initially at $q = 0$ the following trajectory ($\tau \ge 1$)

$$\xi_{\rm c}(\tau) = -\frac{18c}{5}\left(10 + 8\tau^{-3/2} - 15/\tau - 3\tau\right). \tag{17}$$

Thus, $\xi_{\rm c}$ is an effective time-dependent boost that switches on only after shell-crossing, which is clearly non-analytic behaviour; see Section 6 for details. Some indications of that boost, for initial conditions of a distorted Gaussian shape, have been computed numerically in Pietroni (2018); see their fig. 5. We note that the boost $\xi_{\rm c}$ does not only affect the $q = 0$ particle, as shown below.

Having obtained $S_{\rm ZA}$ and $\xi_{\rm c}$, equation (10) can be straightforwardly solved by the method of variation of constants, $\xi_{\rm PSC} = \lambda(\tau)\,\tau + \mu(\tau)\,\tau^{-3/2}$, with boundary conditions provided at shell-crossing, i.e. $\xi_{\rm PSC}(\tau = 1) = \dot\xi_{\rm PSC}(\tau = 1) = v^{\rm (ini)}$, where $v^{\rm (ini)}$ is given in equation (7). See the supplementary material B2 for calculational details. We finally obtain the post-shell-crossing displacement

$$\xi_{\rm PSC}(q,\tau) = \tau v^{\rm (ini)}(q) + \begin{cases} 0; & 0 \le \tau \le \tau_1; \quad \mathbf{S}_{1,2} \\ \delta\xi_{\mathbf{A}}; & \tau_1 \le \tau \le \tau_2; \quad \mathbf{A}_{1,2} \\ \delta\xi_{\mathbf{B}}; & \tau \ge \tau_2; \quad \mathbf{B}_{1,2} \end{cases} \tag{18a}$$

where

$$\delta\xi_{\mathbf{A}} = \frac{{\rm sign}(q)}{180}\frac{D^{5/2}(q,\tau)\,\tau}{8 - q^2 + cq(48 - 11q^2)}, \tag{18b}$$

$$\delta\xi_{\mathbf{B}} = \xi_{\rm c}(\tau) - 3q + \frac{9q\tau}{20}(4 - q^2) + \frac{48}{5}\sqrt{\frac{2}{2 - q^2}}\frac{q\tau^{-3/2}}{8 - q^2} + \frac{9c}{20}\left[64\tau^{-3/2} - \tau q^4 - \frac{16q^4(3q^2 - 4)\tau^{-3/2}}{(1 - q^2/2)^{3/2}(q^2 - 8)^2} - 96\tau_2^{1/2}/\tau^{3/2} + 32\tau_2^{3/2}/\tau^{3/2} - 24\tau(1 - 1/\tau_2)^2\right]. \tag{18c}$$

The resulting map $x_{\rm PSC}(q,\tau) = q + \xi_{\rm PSC}(q,\tau)$ is shown in the top panel of Fig. 1. For convenience, in that figure we have shaded the ascending ($\mathbf{A}_{1,2}$, yellow) and descending ($\mathbf{B}_{1,2}$, blue) multistream branches, while single-stream regions ($\mathbf{S}_{1,2}$) have no shading.

6 SINGULARITIES IN SPACE AND TIME

Starting from the instant of first shell-crossing, some CDM particles are directly exposed to infinite densities at their current positions. We show that the displacements of those exposed particles cannot be represented by convergent spatial or temporal Taylor series, which directly implies that standard perturbative techniques break down. For this we identify the rational singularity exponents λ, which indicate the integer perturbation order $n := \lceil \lambda \rceil$ at which the nth derivative of the displacement, i.e. its Taylor coefficient, blows up.

Singularities in the displacement (18) could originate from two distinct sources, either by (a) explicit non-analytic features within the piecewise defined branches of the map, and/or by (b) discontinuities that arise when 'glueing' the branches together. Related to (a), it is easily checked that the only non-analyticity within the branches arises when $D(q, \tau)$ vanishes (equation 14), which occurs at $\tau = \tau_1$. Related to (b), two other singularities are revealed at τ_2.

To identify the (a)-type singularity it suffices to limit ourselves to $c = 0$. Indeed, a vanishing discriminant D is achieved by freezing the space dependence in D and investigating small discrepancies $\delta\tau > 0$ around τ_1 from above. Taylor-expanding the term with the discriminant around $\delta\tau$ then leads to a $\delta\tau^{5/2}$ singularity. Thus, the displacement behaves locally as $\propto(\tau - \tau_1)^{5/2}$, implying that its third time derivative blows up at τ_1. Similarly, by freezing the time and varying q, one finds spatial singularities at $q_{\mathrm{comax/comin}}$ with exponent 5/2. Physically, what happens is that a spectator particle near $q_{\mathrm{comax/comin}}$ crosses a caustic at the current position.

The (b)-type singularities are expected to occur at τ_2. One of those singularities stems from glueing the ascending and descending multistream branches together, for which purpose it suffices to set $c = 0$. Taylor-expanding around small temporal discrepancies near τ_2, we find that the third-order time derivative flips sign, indicating that the third derivative of ξ is discontinuous, thereby marking a singularity of $\xi \sim (\tau - \tau_2)^3\,\Theta\,(\tau_2 - \tau)$. Similarly, we find that the third spatial derivative of the map is also discontinuous, thus implying spatial singularities near $q_{\mathrm{min/max}}$ of exponent 3.

Lastly, a non-trivial singularity originates from ξ_{c} (equation 17), which is driven by a force imbalance (from $c \neq 0$ in equation 7); this manifests itself through the loss of analyticity at the first shell-crossing, thereby resulting in a dynamical phase transition due to a broken symmetry in the multistreaming force. Indeed, the boost ξ_{c} 'switches' from off to on ($\propto\delta\tau^3$) once multistreaming develops (right-hand panel in Fig. 2). Consequently, a particle that is initially at $q = 0$ will remain there until the first shell-crossing at $\tau = 1$, but then the first time-derivative of its acceleration receives a non-analytic contribution, jumping from 0 to a finite number.

The (a)-type and first (b)-type singularities are shown in the first panel of Fig. 2 ($c = 0$), while the second (b)-type singularity is displayed in the third panel, for $c = 0.1$. We confront these findings against 1D numerical (N-body) simulations that determine the exact particle forces using an efficient sorting algorithm (for a similar implementation however in a non-periodic set-up, see Colombi & Touma 2014). The results of our simulations are marked by dots in Fig. 2. The respective 1D code, which we make publicly available,[1] solves equation (1) with a symplectic time-integrating scheme. Initial conditions are provided by the ZA using equation (7) in a periodic box for $x, q \in [-\pi, \pi]$ (physical units can be trivially restored in the code if needed). Runs were performed with 10^4 CDM particles and time-steps, though for detecting the singularity stemming from ξ_{c}, temporal and spatial resolutions of up to 10^5 have been used.

[1] https://bitbucket.org/ohahn/cosmo_sim_1d

7 CONCLUSIONS

Associated to the known shell-crossing singularities in the CDM density, we have identified three non-differentiable acceleration features. These features imply non-analytic behaviour as derivatives in the phase–space blow up; therefore, any analytical technique that solves for the CDM dynamics by using temporal or spatial perturbative expansions will break down at shell-crossing.

Two of those singularities are of local origin and appear either when particles enter a multistreaming region, or when particles are directly involved in the density caustic (Fig. 1 and first panel in Fig. 2). Yet, a third singularity is of global origin emerging from a boost in the theory, $\xi_{\mathrm{c}}(\tau)$, needed to establish momentum conservation in asymmetric collapse scenarios (second and third panels in Fig. 2). In numerical simulations, by contrast, $\xi_{\mathrm{c}}(\tau)$ appears implicitly by preserving the fundamental conservation laws for Vlasov–Poisson.

Why are the reported singularities relatively so weak? Vlasov–Poisson is intimately linked to a Hamiltonian formulation and is, therefore, constrained by Liouville's theorem (phase–space incompressibility), which guarantees that perfectly CDM is devoid of any disruptions in the position and velocity space (central panel in Fig. 2). One can show that in the generic case of initial data, which do not possess parity invariance ($c \neq 0$ in equation 7), any attempt to construct solutions that ignore $\xi_{\mathrm{c}}(\tau)$ will lead to severe disruptions of the phase–space, thereby violating phase–space incompressibility.

A straightforward yet challenging extension to our work is to exploit the singularity theory in quasi-1D, where departures from 1D are perturbatively small, thus providing a bookkeeping parameter (cf. Rampf & Frisch 2017). Generalizations to 3D are feasible as well, by using higher order LPT (Zheligovsky & Frisch 2014; Rampf, Villone & Frisch 2015; Matsubara 2015; Rampf & Hahn 2020), and providing boundary conditions at shell-crossing, especially for trigonometric initial conditions, where fast Fourier transforms can be avoided (cf. Saga et al. 2018). In this work, we have provided the stepping stones for such avenues; indeed, equations (1)–(3) are trivially generalized to arbitrary dimensions.

A full-fledged theory for the large-scale structure has the potential to advance its theoretical predictions. For example, the theory can determine inputs for heavily used effective theories of the large-scale structure (e.g. Baumann et al. 2012; Porto, Senatore & Zaldarriaga 2014). Indeed, such effective theories incorporate shell-crossing and multistreaming effects through counter terms (with a priori unknown time dependence), which are usually estimated from N-body simulations.

Finally, the Vlasov–Poisson equation applies also when the gravitational field gets replaced by an electrostatic (repulsive) field. One direct application of our theory is the bump-on-tail instability in which a beam of charged particles moves in a background neutral plasma (e.g. O'Neil, Winfrey & Malmberg 1971; Lesur & Diamond 2013; Escande et al. 2018). Indeed, apart from minor adaptions (e.g. sign change of charge), our evolution equations are identical with the one of O'Neil et al. (1971) in the continuous limit. Generalizations to multiple cold beams or to the warm case are straightforward too (see e.g. Carlevaro et al. 2015), and could provide significant insights to the development of instabilities in plasma physics.

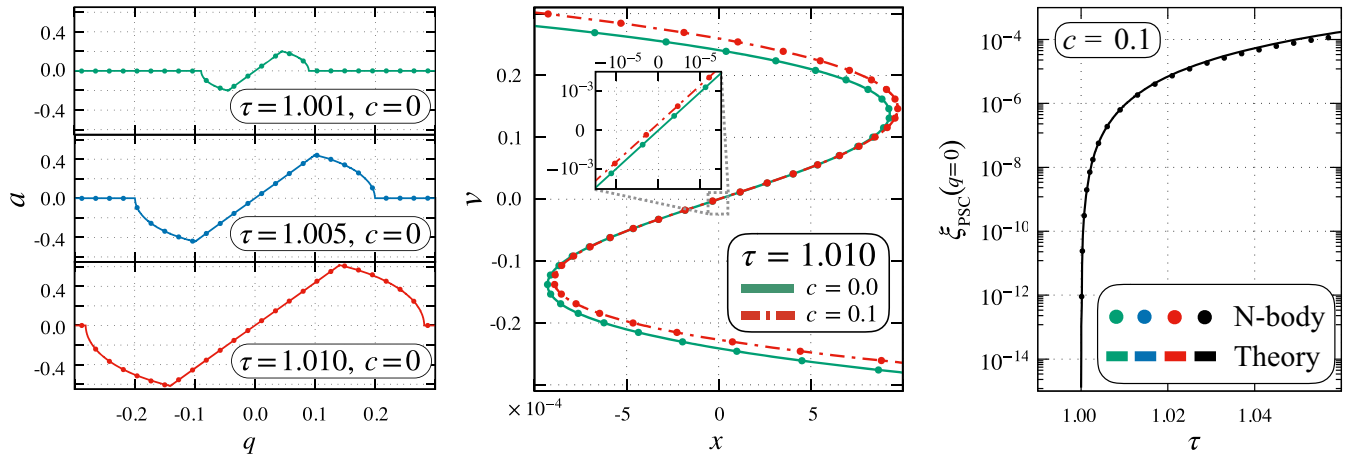

Figure 2. Results of theory (solid or dot–dashed lines) against numerical simulations (dotted; only every 30th data point shown) shortly after the first shell-crossing ($\tau = 1$). The left-hand panel shows the acceleration $a := \ddot{x}_{\rm PSC} = \ddot{\xi}_{\rm PSC}$ as a function of the initial position q for $c = 0$, displaying four non-differentiable sharp features and thereby unveiling singular dynamics (theory and numerics agree almost perfectly). The central panel shows the phase–space shortly after shell-crossing, for $c = 0$ (green) and $c = 0.1$ (red); it involves a slight shift of the particles in the centre of the multistream regime for $c \neq 0$ when the force is asymmetrical. The rightmost panel shows the same effect as a function of time, for the particle that was initially at $q = 0$. The results depicted here cannot be predicted by the ZA; see the supplementary material E for details, including comparisons between ZA and PSC theory as well as late-time results.

ACKNOWLEDGEMENTS

We thank Patrick Diamond, Massimo Pietroni, Zachary Slepian, and Matias Zaldarriaga for useful discussions. CR acknowledges funding from the People Programme (Marie Skłodowska-Curie Actions) of the European Union's Horizon 2020 Programme under Grant Agreement No. 795707 (COSMO-BLOW-UP). UF acknowledges financial support from the Université Côte d'Azur under Grant Agreement No. ANR-15-IDEX-01 (2018–2019). OH acknowledges funding from the European Research Council (ERC) under the European Union's Horizon 2020 research and innovation programme (Grant Agreement No. 679145, project 'COSMO-SIMS').

DATA AVAILABILITY

The code to perform *N*-body simulations in 1D is freely available at https://bitbucket.org/ohahn/cosmo_sim_1d. The data underlying this article will be shared on reasonable request to the corresponding author.

REFERENCES

Arnol'd V. I., 1980, Mathematical Methods of Classical Mechanics. Springer, New York
Arnold V. I., Shandarin S. F., Zeldovich I. B., 1982, Geophys. Astrophys. Fluid Dyn., 20, 111
Baumann D., Nicolis A., Senatore L., Zaldarriaga M., 2012, J. Cosmol. Astropart. Phys., 2012, 051
Bernardeau F., Colombi S., Gaztañaga E., Scoccimarro R., 2002, Phys. Rep., 367, 1
Bouchet F. R., Juszkiewicz R., Colombi S., Pellat R., 1992, ApJ, 394, L5
Buchert T., 1992, MNRAS, 254, 729
Buchert T., Götz G., 1987, J. Math. Phys., 28, 2714
Carlevaro N., Falessi M. V., Montani G., Zonca F., 2015, J. Plasma Phys., 81, 495810515
Colombi S., 2015, MNRAS, 446, 2902
Colombi S., Touma J., 2014, MNRAS, 441, 2414
Ehlers J., Buchert T., 1997, Gen. Relativ. Gravit., 29, 733
Escande D. F., Bénisti D., Elskens Y., Zarzoso D., Doveil F., 2018, Rev. Mod. Plasma Phys., 2, 9
Heckmann O., Schücking E., 1955, Z. Astrophys., 38, 95
Lesur M., Diamond P. H., 2013, Phys. Rev. E, 87, 031101
Matsubara T., 2015, Phys. Rev. D, 92, 023534
Melott A. L., Shandarin S. F., 1989, ApJ, 343, 26
Novikov E. A., 1969, Sov. J. Exp. Theor. Phys., 30, 512
O'Neil T. M., Winfrey J. H., Malmberg J. H., 1971, Phys. Fluids, 14, 1204
Pietroni M., 2018, J. Cosmol. Astropart. Phys., 2018, 028
Porto R. A., Senatore L., Zaldarriaga M., 2014, J. Cosmol. Astropart. Phys., 2014, 022
Rampf C., 2019, MNRAS, 484, 5223
Rampf C., Buchert T., 2012, J. Cosmol. Astropart. Phys., 2012, 021
Rampf C., Frisch U., 2017, MNRAS, 471, 671
Rampf C., Hahn O., 2020, MNRAS, 501, L71
Rampf C., Villone B., Frisch U., 2015, MNRAS, 452, 1421
Saga S., Taruya A., Colombi S., 2018, Phys. Rev. Lett., 121, 241302
Taruya A., Colombi S., 2017, MNRAS, 470, 4858
Taylor A. N., Hamilton A. J. S., 1996, MNRAS, 282, 767
Zel'dovich, Ya. B., 1970, A&A, 500, 13
Zheligovsky V., Frisch U., 2014, J. Fluid Mech., 749, 404

SUPPORTING INFORMATION

Supplementary data are available at *MNRASL* online.

Figure S1. The boost $\xi_c(\tau)$ for different counter terms.
Figure S2. Analysis of the involved integrands in $S_{\rm ZA}$.
Figure S3. The multistreaming force at the PSC refinement level.
Figure S4. Late-time evolution of the boost $\xi_c(\tau)$.
Figure S5. Late-time evolution of the phase–space with $c = 0.1$.
Figure S6. Late-time evolution of the phase–space with $c = 0.0$.

Please note: Oxford University Press is not responsible for the content or functionality of any supporting materials supplied by the authors. Any queries (other than missing material) should be directed to the corresponding author for the article.

This paper has been typeset from a TEX/LATEX file prepared by the author.